颗粒度对 E4303 电焊条性能影响

顾玲燕[1]，　徐越兰[1]，　张　霞[2]，　汤志宁[2]

（1. 南京理工大学 材料科学与工程系，南京　210094；
2. 南京林肯电气有限公司，南京　210019）

顾玲燕

摘　要：以 E4303 电焊条药皮配方中中碳锰铁合金为研究对象，取三种不同颗粒度的中碳锰铁制备 E4303 电焊条。对制备的电焊条分别进行了主要焊接工艺性能测试、熔敷金属的微观组织观察、熔敷金属化学成分分析和熔敷金属冲击性能试验。结果表明，加入纳米级中碳锰铁的电焊条电弧稳定性优良；纳米颗粒增加了晶粒形核的核心，起到了细化晶粒的作用；纳米颗粒烧损严重，减弱了中碳锰铁合金的脱氧、脱硫和渗合金效果，使熔敷金属内产生弥散氧化夹渣，导致冲击韧性降低。

关键词：电焊条；中碳锰铁；颗粒度
中图分类号：TG115.28　　文献标识码：A　　文章编号：0253－360X(2008)10－0050－04

0　序　　言

纳米材料作为近年来科学上的重大发现之一，已成为许多学科研究的热点。赵秀娟等人[1,2]以纳米 W-Fe/C 为主要原料制备堆焊焊条，改善了熔滴过渡形式和电弧稳定性，焊缝组织中粗大的树枝状碳化物被改变为均匀细小的组织，增加了 η 相在基体中的含量，提高了堆焊焊缝硬度。在电焊条配方设计中，随着药皮组分颗粒度的细化，对电焊条综合性能的影响显而易见。

针对 E4303 电焊条中铁合金——中碳锰铁的颗粒度与电焊条各种性能的相关性展开分析研究。

1　试验方法

1.1　中碳锰铁颗粒大小的选择

用酒精溶解和分离中碳锰铁粉末，选择微米级和纳米级两个粒度范围，在电子显微镜下其颗粒形貌如图 1 和图 2 所示。

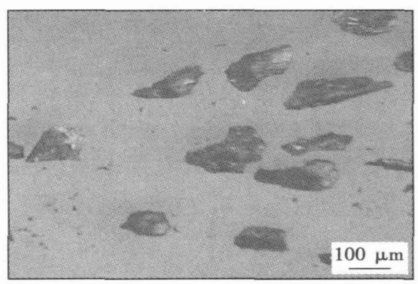

图 1　中碳锰铁微米粉末

Fig. 1　Medium carbon ferromanganese micron powder

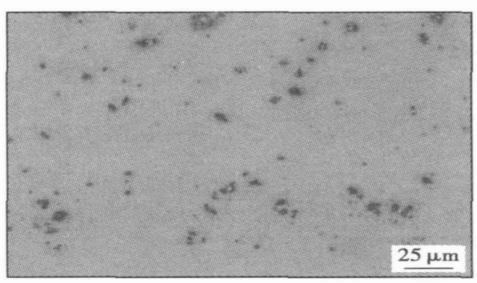

图 2　中碳锰铁纳米粉末

Fig. 2　Medium carbon ferromanganese nano powder

1.2　焊条的制备与熔敷金属的取样

以 H08A 为焊芯，采用钛钙型药皮配方，中碳锰铁按表 1 粒度加入，在 25 t 小型油压机上分别压制 3 组，每组 10 根，共 30 根，并按规定工艺烘干备用。

参照国家标准 GB/T5117－1995 相关内容，制取熔敷金属试样。

1.3　焊条性能测试项目及设备

按照原机械部标准 JB/T8423－1996 进行断弧长度试验。

在 OLYMPUS 光学显微镜下观察熔敷金属金相

收稿日期：2007－12－18

表 1　焊条配方

Table 1　Electrode formula

编号	焊条
1	配方其它成分＋生产用中碳锰铁粉末
2	配方其它成分＋微米级中碳锰铁粉末
3	配方其它成分＋纳米级中碳锰铁粉末

组织；在 QUANTA －200 型电子扫描电镜下进行熔敷金属夹杂物能谱成分扫描。

采用化学分析方法测试熔敷金属化学成分。

在 JB30B 冲击试验机上对熔敷金属进行－20 ℃V 形缺口冲击韧性试验。

2　试验数据及分析

2.1　不同颗粒度断弧长度数据分析

焊接工艺参数为焊接电流 170～190 A，电弧电压 60～80 V，试验数据见表 2。

表 2　断弧长度（mm）

Table 2　Length of broken arc

编号	第一根 L_1	第二根 L_2	第三根 L_3	平均断弧长度 L_0
1	17.0	16.0	17.0	16.7
2	19.0	16.0	14.0	16.3
3	20.5	14.5	16.5	17.2

根据 1989 年国内 E4303 焊条产品质量评比实施细则中的断弧长度评分标准[3]，1，2 号焊条的得分为 0.5 分，3 号焊条的得分为 1 分。

药皮熔点的高低决定于药皮组成物的种类和粒度，药皮组成物的熔点越高，粒度越大，药皮的熔点也越高。药皮熔点过高，易形成长套筒，导致电弧过长而易于熄灭[4]。纳米粉末具有粒度小，表面活性好，熔点低的特性[5]。因此，加入纳米级中碳锰铁后，可使药皮熔点有所下降，减小药皮套筒长度，使焊条断弧长度增加，电弧稳定性变优。而微米级中碳锰铁并不具有纳米材料的性能，断弧长度反而减小，电弧稳定性变差。

2.2　熔敷金属微观组织观察

考虑到焊缝组织的不均匀性，在熔敷金属试样横断面基本相同的部位，选择三个点 A，B，C 进行相同点的微观组织对比观察，选点部位及微观组织分别见图 3 和图 4 所示[6]。

同样由于纳米材料粒度小，表面活性好，熔点低，焊条能更快的燃烧，过渡到焊缝中形成较多的形核核心，并均匀的扩散到熔池中[7]，因此，加入纳米级中碳锰铁的焊条形成了较细小均匀的晶粒，而加入微米级中碳锰铁的焊条形成的晶粒较为粗大，也不均匀，块状与片状先共析铁素体分布于原奥氏体晶间，晶内为魏氏体组织铁素体与珠光体。

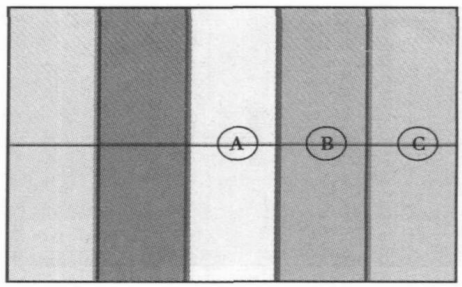

图 3　金相观测位置点

Fig 3　Observed position of metallographic

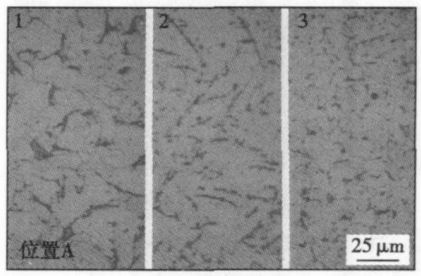

(a) 1，2和3试样位置A处组织对比

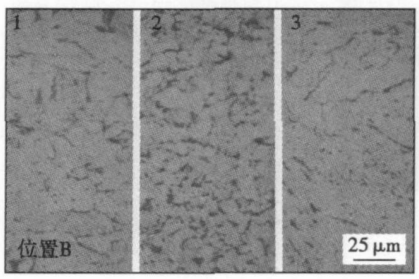

(b) 1，2和3试样位置B处组织对比

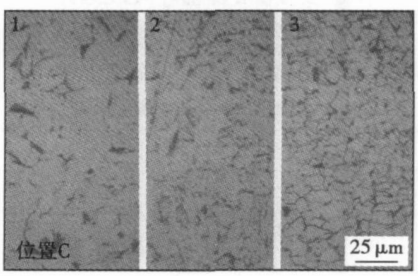

(c) 1，2和3试样位置C处组织对比

图 4　熔敷金属微观组织

Fig. 4　Microstructure of deposited metal

2.3　扫描电镜能谱成分分析

对熔敷金属试样进行了不同形态夹渣物（图 5）成分分析，数据见表 3。

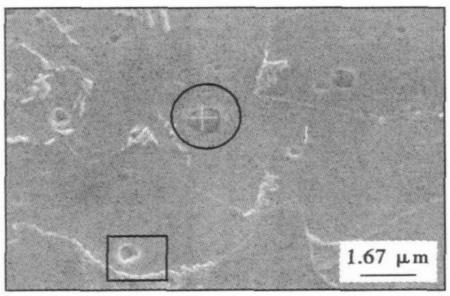

(a) 1号试样夹渣物形态

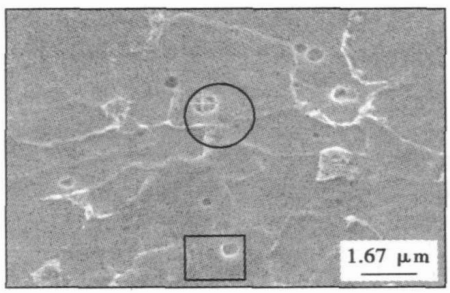

(b) 2号试样夹渣物形态

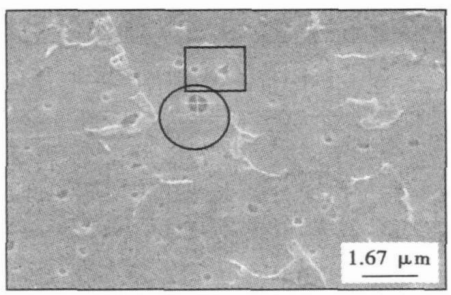

(c) 3号试样夹渣物形态

图 5 夹渣形态

Fig. 5 Form of slag inclusions

表 3 不同形态夹渣成分(质量分数, %)

Table 3 Component of different slag

夹渣成分	1		2		3	
	圆	方	圆	方	圆	方
SiK	22.5	10.8	17.8	16.1	18.2	7.5
SK	0.9	1.6	0.9	0.7	—	—
TiK	3.2	—	1.4	—	3.3	—
MnK	32.8	6.9	12.7	6.9	17.5	1.5
FeK	10.3	66.4	43.1	58.0	36.1	83.6

由图 5, 表 3 可见, 随中碳锰铁颗粒度的细化, 特别是加入纳米级中碳锰铁的焊条熔敷金属, 晶界明显增多, 晶粒细化。同时, 夹渣亦随着颗粒的细化呈现数量增加且弥散分布的趋势, 对不同夹渣形貌进行电子探针分析后证实, 圆形夹渣主要为硅和锰氧化物, 方形夹渣为铁的氧化物。

2.4 化学成分与冲击试验

三种焊条熔敷金属化学成分见表 4。

表 4 熔敷金属化学成分(质量分数, %)

Table 4 Chemical component of deposited metal

编号	Mn	S	C	Si	P	Fe
1	0.43	0.18	0.073	0.13	0.007	余量
2	0.40	0.20	0.077	0.13	0.010	余量
3	0.38	0.22	0.070	0.13	0.007	余量

表 4 数据表明, 中碳锰铁颗粒度的细化使得焊条熔敷金属的锰成分含量下降。一般来说, 增大焊条药皮中合金剂的颗粒度, 可减小表面积, 焊接过程中可减少氧化损失, 提高合金过渡系数。在 E4303 焊条中加入微米级和纳米级中碳锰铁合金粉末后, 不同程度的减小了合金剂的颗粒度, 增大了表面积, 从而增加了氧化损失, 使中碳锰铁随着颗粒度的减小烧损严重[8], 合金过渡系数下降。

3 种电焊条的熔敷金属在 −20 ℃下的 V 形缺口冲击吸收功数据见表 5。

表 5 熔敷金属的冲击吸收功(J)

Table 5 Impact toughness of deposited metal

编号	冲击吸收功 $A_{KV(-20\ ℃)}$						
	1	2	3	4	5	6	7
1	76	77	69	76	81	80	76
2	81	82	87	84	84	75	82
3	51	67	59	68	66	83	66

虽然熔敷金属的冲击吸收功均符合国家标准的要求(≥27 J), 但由于加入纳米级中碳锰铁的焊条熔敷金属中较高的氧化物和硫化物含量, 使熔敷金属的冲击吸收功有所降低。

3 结 论

(1) 加入纳米级中碳锰铁后的电焊条电弧稳定性变优, 加入微米级中碳锰铁的焊条其电弧稳定性变差。

(2) 纳米级中碳锰铁的加入增加了晶粒形核的核心, 起到细化晶粒的作用, 微米级中碳锰铁加入反而使晶粒变得不均匀。

(3) 纳米级中碳锰铁颗粒烧损严重, 减弱了合金的冶金脱硫和脱氧作用, 过多且弥散的氧化夹渣, 是纳米级试样冲击韧性降低的主要原因。

(4) 在保证已有的良好工艺性能和较细晶粒的基础上, 提高中碳锰铁在配方中的相对含量及合适的纳米中碳锰铁的比例, 解决纳米中碳锰铁烧损严重的问题, 保证足够的合金过渡量和较好的脱氧、脱

[下转第 56 页]

3 结 论

(1) 在温度循环载荷下, 由于芯片、焊点、基板的 α_l 不匹配而导致焊点内部产生内应力应变, 焊点的等效蠕变应变最大值出现在芯片下的边缘焊点上表面。

(2) 热循环的开始阶段, 应力松弛现象显著。塑性应变和蠕变应变在时间历程处理过程中, 以阶梯状累积增加。迟滞环进行周期性变化, 并趋于稳定。

(3) 分别借助于 Solomon 模型和 Shine and Fox 模型, 算出焊点疲劳寿命, 再进一步基于塑性应变和蠕变应变的疲劳寿命方程, 得出焊点失效疲劳循环为 1 648 周次。

参考文献:

[1] 肖小清, 何小琦, 恩云飞, 等. 倒装芯片焊点可靠性的有限元模拟法综述[J]. 电子工艺技术, 2006, 27(4): 201—204.

[2] 李晓延, 王志升. 倒装芯片封装结构中SnAgCu 焊点热疲劳寿命预测方法研究[J]. 机械强度, 2006, 28(6): 893—898.

[3] Lau J H, Pan S H. Creep behaviors of flip chip on board with 96.5Sn3.5Ag and 100In lead-free solder joints[J]. The International Journal of Microcircuits and Electronic Packaging, 2001, 24(1): 1063—1674.

[4] Kim J W, Kim D G, Hong W S. Evaluation of solder joint reliability in flip-chip packages during accelerated testing[J]. Journal of Electronic Materials, 2005, 34(12): 1550—1557.

[5] Tee T Y, Kho C L, Yap D, *et al*. Reliability assessment and hygro-swelling modeling of FCBGA with no-flow underfill[J]. Microelectronics Reliability, 2003, 43(5): 741—749.

[6] 王国忠, 陈 柳, 程兆年. 电子封装 SnPb 钎料和底充胶的材料模型及其应用[J]. 机械工程学报, 2000, 36(12): 33—38.

[7] Lau J, Dauksher W. Reliability of an 1657 CCGA (ceramic column grid array) package with 95.5Sn3.9Ag0.6Cu lead-free solder paste on PCBS(printed circuit boards)[J]. Journal of Electronic Packaging, 2005, 127(2): 96—105.

[8] Lau J H, Pan S H, Chang C. Creep analysis of wafer level chip scale package (WLCSP) with 96.5Sn-3.5Ag and 100In lead-free solder joints and microvia build-up printed circuit board[J]. Journal of Electronic Packaging, 2002, 124(2): 69—76.

[9] Perkins A, Sitaraman S. Vibration-induced solder joint failure of a eramic column grid array(CCGA) package[C] // Electronic Components and Technology Conference, Atlanta, GA, USA, 2004, 1271—1278.

[10] Che F X, Pang J H L. Thermal fatigue reliability analysis for PBGA with Sn-3.8Ag-0.7Cu solder joints[C] // Electronics Packaging Technology Conference, Singapore, 2004, 787—792.

[11] 马 鑫, 钱乙余, 吉田综仁. 表面组装焊点内部应力—应变场的数值模拟(Ⅰ)[J]. 中国有色金属学报, 2000, 10(3): 404—410.

[12] Cai X, Chen L, Zhang Q, *et al*. Quantitative mechanism of significant benefits of underfill in flip-chip assemblies[J]. Journal of Electronic Packaging, 2003, 125(1): 84—92.

[13] Solomon H. Fatigue of 60/40 solder[J]. Transaction on Components, Hybrids and Manufacturing Technology, 1986, 9(4): 423—432.

[14] Pang J H L, Seetoh C W, Wang Z P. CBGA solder joint reliability evaluation based on elastic-plastic-creep analysis[J]. Journal of Electronic Packaging, 2000, 122(3): 255—261.

[15] Yeo A, Lee C, Pang J H L. Flip chip solder joint fatigue analysis using 2D and 3D FE models[C] // 5th International Conference on Thermal and Mechanical Simulation and Experiments in Micro-electronics and Micro-System, Singapore, 2004: 549—555.

作者简介: 盛 重, 男, 1984 年出生, 硕士研究生。主要从事微电子焊接及无铅钎料研究。发表论文 2 篇。

Email: orochiai@126.com

[上接第 52 页]

硫效果, 具有进一步的研究价值。

参考文献:

[1] 姚上卫. 纳米技术在焊接领域的应用[J]. 焊接学报, 2007, 28(3): 109—112.

[2] 赵秀娟, 杨德新, 陈春焕. 纳米复合粉末制D707 焊条[J]. 硬质合金, 2003, 20(2): 76—79.

[3] 文 景, 文援兰. 电焊条研制技术[M]. 北京: 国防科技大学出版社, 2001.

[4] 张清辉. 焊接材料研制理论与技术[M]. 北京: 冶金工业出版社, 2002.

[5] 张立德. 纳米材料[M]. 北京: 化学工业出版社, 2000.

[6] 秦国友. 定量金相[M]. 四川: 四川科学技术出版社, 1987.

[7] 陈伯蠡. 金属焊接性基础[M]. 北京: 机械工业出版社, 1982.

[8] 张子荣, 李升鹤. 电焊条[M]. 北京: 机械工业出版社, 1996.

作者简介: 顾玲燕, 女, 1984 年出生, 硕士研究生。主要研究方向是焊接新工艺和新型焊条开发研究。

Email: glyjq@yahoo.com.cn

ZHOU Xiaoling, SUN Jianchun (School of Materials Science & Engineering, Chongqing University, Chongqing 400030, China). p37—40

Abstract: Surface self-nanocrystallization (SSNC) by means of high energy shot peening (HESP) was applied to produce nanostructures on the ends of TA17 titanium alloy and 0Cr18Ni9Ti stainless steel bars, nanostructured surface layers were formed on the ends of samples. Making treated surfaces as interface, TA17 and 0Cr18Ni9Ti bars were bonded by impact pressure diffusion bonding (IPDB) on Gleeble—1500D tester. Joints were tested on tensile testing machine, the fractures and microstructures on the longitudinal section of joints were researched. Results shown that the maximum strength is about 384.0 MPa, brittle fracture is generated as the joints were tested, and the microhardness are varied with microstructures on the longitudinal section of joint.

Key words: surface self-nanocrystallization; titanium alloy; stainless steel; diffusion bonding; impact pressure

Stress distribution in Al_2O_3-TiC/1Cr18Ni9Ti diffusion bonded joint SHEN Xiaoqin[1,2], LI Yajiang[1], Puchkov U A[3], WANG Juan[1] and HUANG Wanqun[1] (1. Key Lab of Liquid Structure and Heredity of Materials, Ministry of Education, Shandong University, Jinan 250061, China; 2. School of Mechatronics, Shandong Jianzhu University, Jinan 250101, China; 3. Materials Science Department, Bauman Moscow State Technical University, Moscow 105005, Russia). p41—44

Abstract: The stress distribution of Al_2O_3-TiC/1Cr18Ni9Ti diffusion bonded joint was calculated using the finite element method and the effects of bonding temperature, pressure and interlayer on the stress distribution were studied. The results indicate that the axial stress and the shear stress both change greatly near the sample edge, which uniform near the center. The greatest shear stress occurs at the Al_2O_3-TiC/interlayer interface. The greatest axial tensile stress shifts from the ceramic side on the sample edge to the steel side near the edge and the value increases with the temperature decreasing. The axial compressive stress increases when the bonding temperature reduces. The increasement of the pressure can reduce the maximal axial tensile stress and improve the compressive stress. The change of the pressure has little effect on the shear stress. Both of the axial tensile stress and the shear stress decrease with Ti-Cu-Ti interlayer compared with Ti interlayer.

Key words: Al_2O_3-TiC; stainless steel; diffusion bonding; stress

Numerical simulation of friction stir welding for aluminum alloy railway carriage manufacturing ZHU Wenfeng[1], XU Chun[2] (1. School of Mechanical Engineering, Tongji University, Shanghai 200092, China; 2. Shanghai Institute of Technology, Department of Material, Shanghai 200235, China). p45—49

Abstract: High speed railway (HSR) uses aluminum hollow extrusions as new material and friction stir welding (FSW) is an innovative solid phase welding for such carriage manufacturing. Considering both the heat generation from tool shoulder friction and plastic deformation near the tool pin, a dual source finite element model of FSW is presented and a variety of weld joint designs are realized which satisfy the feature of FSW for the double skinned extrusion aluminum alloy structure. By ANSYS-APDL based re-exploitation, moving heat sources simulation is realized, and temperature field is obtained during the welding. The calculated results are in good agreement with experimental data, which indicate the model's feasibility and accuracy. It will benefit the digestion & assimilation of domestic-made level HSR vehicle manufacturing technology and provide reference for FSW process parameters optimization.

Key words: dual heat source; friction stir welding; aluminum alloy railway carriage; numerical simulation

Granularity effect to E4303 electrodes' performance GU Lingyan[1], XU Yuelan[1], ZHANG Xia[2], TANG Zhining[2] (1. Department of Materials Science and Engineering, Nanjing University of Science and Technology, Nanjing 210094, China; 2. Nanjing Lin Ken Equipment Limited Liability Company, Nanjing 210005, China). p50—52, 56

Abstract: Three different electrodes with different granularities medium carbon ferromanganese had been studied. The researches include welding technology performance of electrodes, the microstructure of deposited metal, chemical composition and impact toughness of deposited metal. The results showed that by adding nano medium carbon ferromanganese, the arc stability is better, the nano granule can increase nucleation core of crystal which play a role in grain refining, meanwhile the nano grain is burned badly, the deoxidation and desulfidation are weaken, impact toughness of deposited metal is reduced due to the overabundance oxide slag.

Key words: electrode; granularity; medium carbon ferromanganese

Fatigue life prediction for flip chip soldered joints based on creep stain model SHENG Zhong, XUE Songbai, ZHANG Liang, GAO Lili (Coolege of Materials Science and Technology, Nanjing University of Aeronautics and Astronautics, Nanjing 210016, China). p53—56

Abstract: Finite element method was used to simulate the inelastic stress in soldered joints of flip chip, and the results indicated that the maximums of equivalent creep strain and equivalent plastic strain in soldered joint both located at the upper surface of limbic chip. Processing the stress and strain of soldered joints with time, it was indicated that soldered joints had significantly relaxed the stress in the initial stage of circulation, with the accumulated trends of plastic strain and creep strain. With the hysteresis loop of stress-strain, cyclical variation of the loop was observed, and the curve became stable with the cyclic loading of heat. On account of the interaction between plastic strain and creep strain, the solomon model and shine and fox model were utilized to calculate fatigue life of the soldered joints. The simulated results were almost the same with the the practical life.

Key words: finite element method; plastic stain; creep stain; fatigue life

Grain growth in heat affected zone of fine grained titanium alloy WU Wei, GAO Hongming, CHENG Guangfu, WU Lin (State Key Laboratory of Advanced Welding Production Technology, Harbin Institute of Technology, Harbin 150001, China). p57—60, 64

Abstract: Grain growth in coarse grained region of fine grained titanium alloy welded joint was studied, and influences of